Mass enhancement versus Stoner enhancement in strongly correlated metallic perovskites: $LaNiO_3$ and $LaCuO_3$

J.-S. Zhou,* L. G. Marshall, and J. B. Goodenough
Materials Science and Engineering Program/Mechanical Engineering, University of Texas at Austin, Austin, Texas 78712, USA
(Received 14 April 2014; revised manuscript received 13 June 2014; published 30 June 2014)

Measurements of physical properties, including transport and magnetic properties, specific heat, and thermal conductivity, have been performed on high-quality samples of $LaNiO_3$ and $LaCuO_3$ synthesized under high pressure. Some measurements, such as thermoelectric power and magnetic susceptibility, have been made under high pressure. The availability of a complete set of data enables a side-by-side comparison between these two narrowband systems. We have demonstrated unambiguously the mass enhancement due to electron-electron correlations in both systems relative to the recent density functional theory results. Correlations in these narrowband systems also enhance the magnetic susceptibility. Ferromagnetic spin fluctuations give rise to a strong Stoner enhancement in the magnetic susceptibility in the quarter-filled $LaNiO_3$. Although we are able to tune the bandwidth by either chemical substitutions or by applying hydrostatic pressure on $LaNiO_3$, the Stoner enhancement does not lead to the Stoner instability.

DOI: 10.1103/PhysRevB.89.245138 PACS number(s): 71.27.+a, 75.20.−g, 71.30.+h, 72.80.Ga

I. INTRODUCTION

Perovskites $LaNiO_3$ and $LaCuO_3$ exhibit metallic conductivity, which is rarely found in the $3d$ perovskite oxides. Due to electron-electron correlations in these narrowband systems, their magnetic susceptibilities deviate from Pauli paramagnetism, i.e., χ is much enhanced relative to $\chi_p = {\mu_B}^2 N(\varepsilon_F)$ and becomes temperature dependent. Depending on the band filling, the enhancement of magnetic susceptibility is described by either the mass enhancement or Stoner enhancement. A mass enhancement is predicted for a half-filled band, where antiferromagnetic spin-spin interactions should occur, whereas a Stoner enhancement is predicted for a quarter-filled band, where ferromagnetic spin-spin interactions should occur. Quarter-filled $LaNiO_3$ and half-filled $LaCuO_3$ serve as classic examples to demonstrate these two types of enhancement described by Mott in his book *Metal-Insulator Transitions* [1]. Both oxides were synthesized under high pressure and their magnetic properties were measured in the 1970s [2,3]. However, these early measurements were not carried out with a superconducting quantum interference device (SQUID) magnetometer, and their accuracy may be questioned, especially when the magnetic susceptibility is extremely small. Whereas in his book Mott has implied that these two types of enhancements should be identified by comparing the change of the γ and χ relative to their values from band calculation, his assignment of a mass enhancement to $\chi(T)$ of $LaCuO_3$ and a Stoner enhancement to $\chi(T)$ of $LaNiO_3$ was made based on only a comparison of the early data for $\chi(T)$ between these two perovskites. $LaNiO_3$ and $LaCuO_3$ have been continuously studied over time, especially after the discovery of high T_c superconductivity in cuprates in 1986 [4–22]. However, the data available in the literature are not sufficient to conduct a rigorous test of how electron-electron correlations influence physical properties, such as the magnetic susceptibility in these classic systems. In this paper, we report all transport and magnetic properties, thermal conductivity, and the thermodynamics all measured on the same high-quality samples of $LaNiO_3$ and $LaCuO_3$ that have been characterized by a structural study. It is very important to know that the physical properties of these perovskites are extremely sensitive to the crystal structure and chemical stoichiometry. The data analysis and a comparison with the density functional theory (DFT) calculations made recently enable us to distinguish unambiguously the mass enhancement and the Stoner enhancement in these two perovskite systems.

II. EXPERIMENTAL DETAILS

Single-phase, rhombohedral $La_{1-x}Nd_xCuO_3$ ($0 \leqslant x \leqslant 0.5$) samples were prepared under high pressure and high temperature with a belt-type high-pressure facility. The sample and $KClO_3$ separated by yttrium-stabilized ZrO_2 were sealed in a copper crucible with a gold sleeve inside before being loaded into the pressure cell assembly [13]. Although the critical value of oxygen stoichiometry remains to be determined, the rhombhedral phase $LaCuO_3$ transforms to the tetragonal $LaCuO_{3-\delta}$ upon heating to 408 °C [23]. We have found that the rhombohedral phase of $La_{1-x}Nd_xCuO_3$ for x up to 0.3 can be obtained under 6 GPa and 900 °C. The high-pressure products are high-density pellets. The sample is dark brown in color with metallic luster; the color becomes darker as the Nd substitution increases. The rhombohedral $LaNiO_3$ was synthesized under 600 bar oxygen pressure at 1080 °C. The oxygen content was determined to be 3.00 ± 0.01 by thermogravimetric analysis in a 50-50 H_2-Ar atmosphere. The as-made $LaNiO_3$ sample is porous. In order to obtain reliable transport properties, the sample was further treated by the cold-press method; see Ref. [24] for the detailed information. Phase purity of these samples was examined with powder x-ray diffraction (XRD) at room temperature with a Philips X'Pert diffractometer (Cu $K\alpha$ radiation). The XRD data were collected by step-scanning from 15 to 120° in 2θ, with an increment of 0.02° and a counting time of 10 s at each step. The XRD patterns were analyzed by the Rietveld method with the software FullProf. Magnetic properties were measured with a commercial SQUID

*jszhou@mail.utexas.edu

(Quantum Design). The temperature dependence of resistivity was measured with a standard four-probe method by using both a homemade setup and a commercial Physical Property Measurement System (PPMS DynaCool, Quantum Design) from 300 to 2 K. The specific-heat measurements down to 2 K under 0 and 9 T were performed with a two-tau relaxation method in a PPMS DynaCool. The temperature dependence of thermal conductivity was measured with a steady-state method in the temperature range 5–300 K. Both thermal conductivity and thermoelectric power were measured with homemade setups. The magnetization measurement under high pressure was performed with a Be-Cu piston cylinder device that fits the commercial SQUID magnetometer. Under a magnetic field $H = 5000$ Oe, the magnetization signal (in the order of 10^{-4} emu) from the $LaNiO_3$ sample is at the same level as that from the pressure cell. In order to get a clean dipole response from the SQUID magnetometer, which is essential for an accurate measurement of the magnetic moment, the background contribution measured from the device without the sample was subtracted from the total signal in measurements with the sample.

III. RESULTS

Although the model to refine the crystal structure of $LaCuO_3$ and $LaNiO_3$ has been reported in the literature, patterns of powder XRD for $La_{1-x}Nd_xCuO_3$ ($x = 0$, 0.2) and $LaNiO_3$ are shown in Fig. 1 to demonstrate the quality and to provide structural parameters of the samples used in this study. More importantly, the result of $La_{0.75}Nd_{0.25}CuO_3$ is new, which reveals how the structure changes as a small rare earth is substituted at the A site of the perovskite structure. The electronic structure near the Fermi surface in an ABO_3 perovskite is primarily determined by the electron wave functions of the B-O-B array. The perovskite structure can accommodate a geometric factor $t \equiv (A\text{-O})/\sqrt{2}(B\text{-O}) < 1$ by octahedral-site rotations, which reduces the B-O-B bond angle from 180°. For the localized electronic state, the averaged B-O bond length is nearly independent of a change of the t factor [25]; the orbital overlap integral is mainly proportional to the B-O-B bond angle. As shown in Table I, the B-O bond length and the B-O-B bond angle change very little from $LaNiO_3$ and $LaCuO_3$. However, the change of the Cu-O-Cu bond angle is noticeable from $LaCuO_3$ to $La_{0.75}Nd_{0.25}CuO_3$. As shown in the following, this bond angle change can cause obvious changes of the physical properties.

Figure 2 shows a complete set of experimental results for $LaNiO_3$ and $LaCuO_3$; they are shown side by side for comparison. The magnitude of the susceptibility is small for both perovskites. In contrast to the early results [1], $LaNiO_3$ exhibits a $\chi(T)$ that is more temperature dependent than that of $LaCuO_3$. By carefully selecting the high-pressure product of $LaCuO_3$ to avoid microcracks, the resistivity of $LaCuO_3$ in Fig. 2 is about an order of magnitude lower than that reported previously. The excellent conducting properties classify $LaCuO_3$ to a small group of transition-metal perovskites, including ReO_3 [26] and $SrMoO_3$ [27], with very small resistivities in the level of a few micro ohm centimeters. $LaNiO_3$ exhibits a similar metallic conductivity as $LaCuO_3$, but its $\rho(T)$ is about one order higher than that of $LaCuO_3$.

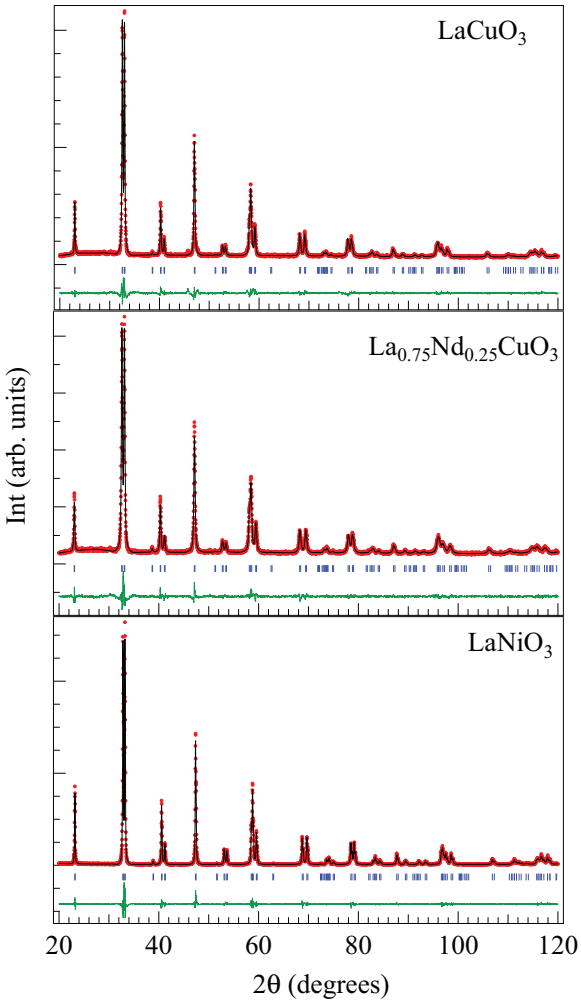

FIG. 1. (Color online) XRD patterns of $LaCuO_3$, $La_{0.75}Nd_{0.25}CuO_3$, and $LaNiO_3$ and results of the Rietveld refinement.

The temperature dependence of thermoelectric power for both perovskites in Fig. 2 can be described qualitatively by the Mott diffusive formula [1] $S = \frac{\pi^2}{3}\frac{k_B^2 T}{e}\frac{dln\sigma(E)}{dE}$, where $\sigma(E)$ is the energy-dependent conductivity ($\sigma = \int \sigma(E)dE$). A smaller magnitude of the derivative $\frac{dln\sigma(E)}{dE}$ might be expected for a half-filled band system like $LaCuO_3$ than that in a quarter filled band system such as $LaNiO_3$. At low temperatures, the linear temperature dependence of S gives way to a hump due to the phonon-drag effect, which is typical in a metal [28]. The presence of the phonon-drag effect requires a modest electron-phonon interaction. If the coupling is too strong it would disturb the lattice dynamics so as to reduce the phonon-drag effect. While the phonon-drag effect is noticeable in $S(T)$ for both perovskites, the magnitude of this effect may be reduced in these narrowband systems. This argument can be further tested by observing the change of $S(T)$ under high pressure. Pressure broadens the bandwidth by increasing the M-O-M bond angle and reducing the M-O bond length, where M is a transition metal, as demonstrated in the structural study of $LaCrO_3$ under high pressure [29]. As shown in Fig. 2, the phonon-drag effect is indeed enhanced progressively under

TABLE I. The structural parameters from Rietveld refinement and fitting results from measurements of physical properties for rhombohedral $LaNiO_3$, $LaCuO_3$, and $La_{0.75}Nd_{0.25}CuO_3$. The calculation of χ_0 and γ have been made based on the DFT results in Ref. [33].

	$LaNiO_3$				$LaCuO_3$				$La_{0.75}Nd_{0.25}CuO_3$			
Space group	R-3c											
Lattice parameter (Å)	5.4574(1),		13.1378(3)		5.49944(5),		13.2172(1)		5.49264(7),		13.1579(1)	
	x	y	z	B_{iso} (Å^2)	x	y	z	B_{iso} (Å^2)	x	y	z	B_{iso} (Å^2)
La(Nd)	0	0	0.25	0.075	0	0	0.25	0.79	0	0	0.25	0.38
M	0	0	0	0.24	0	0	0	0.59	0	0	0	0.22
O	0.545(1)	0	0.25	0.28	0.5403(4)	0	0.25	1.5	0.5500(3)	0	0.25	0.32
M-O (Å)	EXP		1.935				1.9449				1.9437	
	DFT		1.953				1.950					
M-O-M (°)	EXP		165.26				166.89				163.76	
	DFT		163.02				161.96					
Refinement factors	R_p:9.47; R_{wp}:13.3; χ^2:1.59				R_p:4.76; R_{wp}:6.32; χ^2:2.02				R_p:4.68; R_{wp}:6.08; χ^2:1.91			
$\rho = \rho_0 + AT^n$	$A = 1.8 \times 10^{-9}$ $\mu\Omega$ cm/K^2, $n = 2$,				$A = 7.7 \times 10^{-11}$ $\mu\Omega$ cm/K^2, $n = 2$				$A = 3.9 \times 10^{-10}$ $\mu\Omega$ cm/K$^{1.75}$, $n = 1.75$			
χ_0 (emu/mol)	EXP		6.04×10^{-4}				7.74×10^{-5}					
	DFT		5.88×10^{-5}				4.30×10^{-5}					
γ (mJ K^{-2} mol^{-1})	EXP		18.1				5.6					
	DFT		4.3				3.2					
T^* (K)	30				170				N/A			

pressure in both $LaNiO_3$ and $LaCuO_3$. The specific-heat data $C_p(T)$ will be used to extract the electronic contribution γT, which is critical for distinguishing the enhancement in magnetic susceptibility. The thermal conductivity κ for both $LaNiO_3$ and $LaCuO_3$ is higher than in perovskite insulators like $LaCrO_3$ or $LaGaO_3$ [30] because of the electronic contribution in these metallic perovskites. However, the electronic contribution to κ in $LaCuO_3$ as calculated from the electrical conductivity via the Wiedmann-Franz (WF) law is higher than the total κ presented in Fig. 2. It remains unknown why the WF law is violated in $LaCuO_3$.

IV. ANALYSIS AND DISCUSSION

The paramagnetic susceptibility can be generally described by $\chi = \chi_0(1 - aT^2)$ [31], where $\chi_0 = \mu_B^2 N(E_F)$ for a metal. However, contributions from impurity ions and defects are not avoidable; they may become pronounced where the paramagnetic susceptibility from the matrix phase is extremely small. Therefore, we have used $\chi = \chi_0(1-aT^2) + C/T$ to fit the $\chi(T)$ for $LaNiO_3$ and $LaCuO_3$. A similar formula has also been used to fit $\chi(T)$ of $LaNiO_3$ by Sreedhar *et al.* [16]. By comparing with the magnetic susceptibility in the literature, the magnitude of χ in the $LaCuO_3$ sample made by Demazeau *et al.* [2,3] is higher by a factor five than that in Fig. 2, possibly due to the magnetometer used in the early days. All measurements on the $LaNiO_3$ samples by a SQUID magnetometer (Quantum Design) give a relatively flat χ within a very small range around $5*10^{-4}$ emu/mole at high temperatures [16,17]. However, the magnitude of the low-temperature upturn varies from sample to sample made in different groups. This observation justifies application of the formula $\chi = \chi_0(1-aT^2)+C/T$ for separating the intrinsic magnetization from the extrinsic one due to impurities. As shown in Fig. 3, slightly better fits were obtained if the formula $\chi = \chi_0(1 - aT) + C/T$ is used. Nevertheless, the choice of the fitting formula does not influence χ_0 in Table I, the most important parameter for the following analysis.

The temperature dependence of resistivity for both metallic perovskites can be fit by the power law $\rho = \rho_0 + AT^n$. As shown in Fig. 4 for both $LaNiO_3$ and $LaCuO_3$, the $\rho(T)$ at low temperatures fulfills Fermi liquid behavior, i.e., $n = 2$, with high precision. It is remarkable that the ρ versus T^2 curve can be fit linearly up to $T^* \approx 170$ K in $LaCuO_3$. As revealed by the structural study, the Nd substitution reduces the Cu-O-Cu bond angle from 166.9° in $LaCuO_3$ to 163.76° in $La_{0.75}Nd_{.25}CuO_3$. Therefore, the bandwidth is reduced correspondingly. As a result, enhanced correlations make $\rho(T)$ deviate from Fermi liquid behavior. We found that $\rho(T)$ can be fit well by the power law $\rho = \rho_0 + AT^{1.75}$. This result suggests that strong correlations lead the system toward a quantum critical point in the vicinity of a magnetically ordered phase where n will be further reduced to $n = 1.5$ [32]. In contrast, a lower $T^* \approx 30$ K is obtained for $LaNiO_3$. A much higher T^* for $LaNiO_3$ has been reported in the literature [16,17]. However, a surprisingly high resistivity and relatively poor data quality in those measurements make the assignment questionable.

Figure 5 displays the C_p of $LaNiO_3$ and $LaCuO_3$ and the fitting results at low temperatures. A standard formula of specific heat in a solid, $C_p = \gamma T + \beta T^3 + \alpha T^5$ was used in the fitting; the first term is the electronic contribution, and the second and the third are from the lattice. The fitting results are listed in Table I. A relatively higher $\gamma = 18.1$ mJ K^{-2} mol^{-1} in $LaNiO_3$ than that ($\gamma = 5.6$ mJ K^{-2} mol^{-1}) in $LaCuO_3$ is consistent with the prediction from the DFT calculations [33].

Now, we are in the position to discuss the enhancements relative to that from an electron gas on γ and χ_0 due to strong electron-electron correlations. To describe completely the many-body correlations remains a challenge. The modern band calculation technique can include the correlation effect

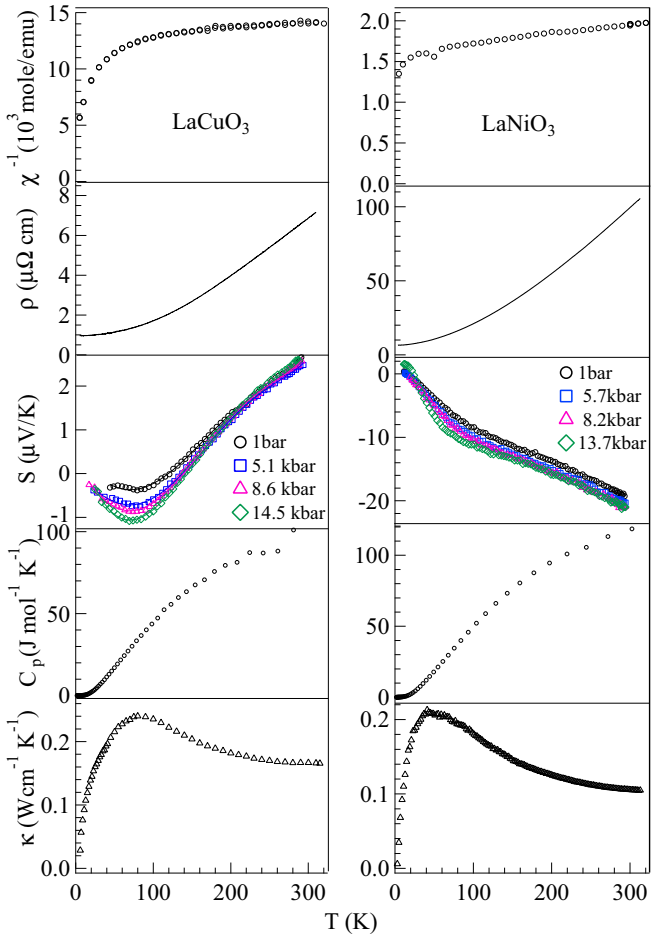

FIG. 2. (Color online) Temperature dependence of the inverse magnetic susceptibility, resistivity, thermoelectric power under different pressures, specific heat, and thermal conductivity for $LaNiO_3$ and $LaCuO_3$. The thermoelectric power data have been previously shown in Refs. [12,21].

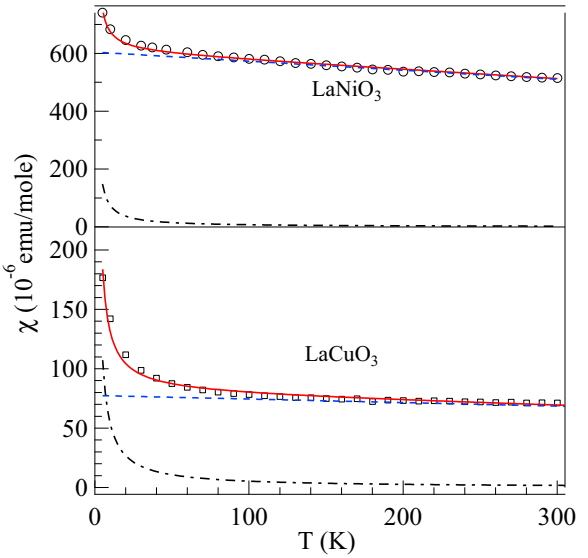

FIG. 3. (Color online) Temperature dependence of magnetic susceptibility of $LaNiO_3$ and $LaCuO_3$ and the fitting results; dashed lines are for the term $\chi_0(1-aT)$, and the dot-dashed lines are for the C/T term, which are decomposed from the curve fitting to the formula $\chi = \chi_0(1-aT)+C/T$.

on the electronic structure to some extent. For example, the mean-field treatment of the Coulomb interactions and the exchange interactions can be covered via the Hartree-Fock (HF) approximation. However, as shown in the Feynman diagram of the energy in a many-body system [34], the HF term is only a part of the whole interaction diagrams, although it is an important term. The more popular DFT calculation starts from the charge density instead of the wave functions. The DFT calculation offers a highly precise description for quasiparticles in a solid. But a free parameter U has to be introduced to account for the Mott transition. The enhancement we are talking about here is the difference between the experimental value and the DFT result. In other words, the enhancement reflects what is still missing in the DFT calculation in terms of electron-electron correlations.

Although there are several band calculations of $LaNiO_3$ and $LaCuO_3$ in the literature, we duplicate here the most recent calculation results by He and Franchini in Fig. 6; they have made the calculations for the entire series of $LaMO_3$ (M = Sc-Cu) [33]. In addition to the band structure, they have also provided the optimized crystal structures. Some of the typical M-O bond lengths and M-O-M angles are included in Table I in order to compare with the structural refinement of the samples used in this work. These results match the experimental values very well. As expected from the band filling of the σ^* band for Ni^{3+} and Cu^{3+}, the Fermi energy is located near the bottom of a broad band in $LaNiO_3$, while it is at the middle of a broader band in $LaCuO_3$. The thermoelectric power S is a measure of the lack of symmetry near E_F in the density of states (DOS). The E_F in $LaNiO_3$ is at the edge of a broad peak in the DOS versus energy, whereas it is at a plateau in $LaCuO_3$. These observations are consistent with a much higher $|S|$ in $LaNiO_3$ than that in $LaCuO_3$. To analyze the enhancement, $N(E_F)$ is needed from the band calculation; it is 1.82 states (electron volt, spin, unit cell) for $LaNiO_3$ and 1.32 states (electron volt, spin, unit cell) for $LaNiO_3$ from the DFT calculation [33]. The $\gamma = \frac{\pi^2}{3}k_B^2 N(E_F)$ and $\chi_0 = \mu_B^2 N(E_F)$ based on the DFT results for $LaNiO_3$ and $LaCuO_3$ are given in Table I.

A Stoner enhancement occurs in a system where the Stoner factor $K_0^2 \equiv 1 - S$ decreases dramatically due to the S factor $S = N(E_F)\Omega U_{\text{eff}}$ approaching 1, where Ω is the atomic volume, $U_{\text{eff}} = \frac{U}{1+\beta(N(E_F))}$, β is a constant [1]. The magnetic susceptibility with Stoner enhancement becomes $\chi = \chi_0(1-aT^2)K_0^{-2}$. On the other hand, Brinkman and Rice [35] have shown that in a narrowband metal with antiferromagnetic spin fluctuations, the specific heat and magnetic susceptibility are equally enhanced due to electron-electron correlations. In his book, Mott has summarized the Stoner enhancement and mass enhancement in the following way: "the Stoner enhancement factor can increase χ without limit but not $d\chi/dT$ or γ, and the mass enhancement in nearly antiferromagnetic metals enhance all χ, γ and $d\chi/dT$." However, this statement is no longer accurate. The γ from experiment is much enhanced relative to the γ_{DFT} due to electron-electron correlations even in a system, where the S factor approaches 1. In other

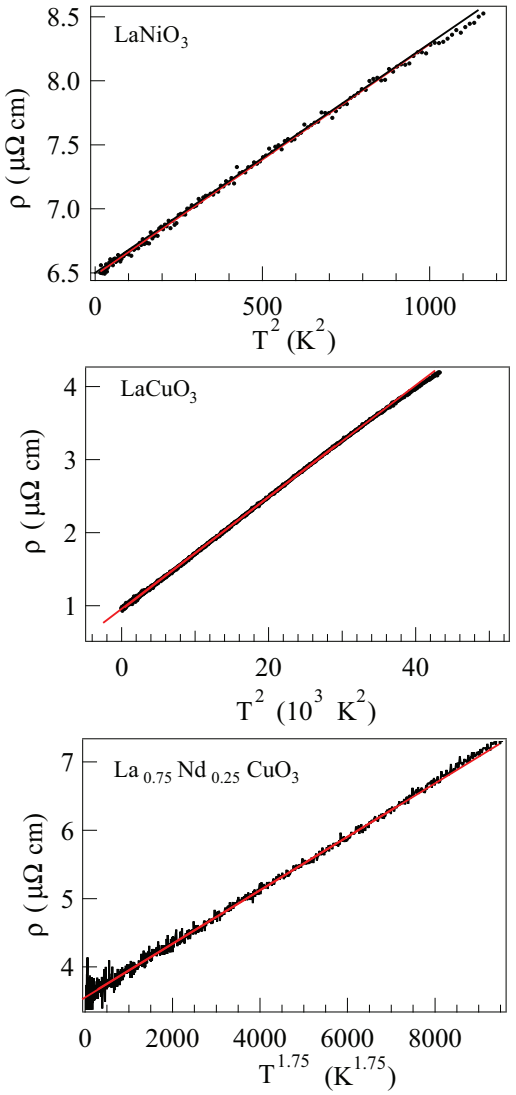

FIG. 4. (Color online) Plot of resistivity versus T^2 for $LaNiO_3$ and $LaCuO_3$ and the plot of resistivity versus $T^{1.75}$ for $La_{0.75}Nd_{0.25}CuO_3$. Lines inside the curves are results of linear fitting.

words, electron-electron correlations and ferromagnetic spin fluctuations in a partially filled band can coexist in a narrow-band system. $LaNiO_3$ offers such an example, where ratios $\gamma/\gamma_{\rm DFT} = 4.2$ and $\chi/\chi_0 = 10.3$ are obtained. In comparison, much smaller ratios $\gamma/\gamma_{\rm DFT} = 1.8$ and $\chi/\chi_0 = 1.9$ are obtained for $LaCuO_3$ where only the mass enhancement is applicable in this half-filled band metal and electron-electron correlations are much weaker than those in $LaNiO_3$. Therefore, it is clear that electron-electron correlations in a narrowband system enhance both γ and χ, but an additional enhancement is applied to χ if the S factor in the system approaches 1.

A recent photoemission result on a single-crystal thin film sample of $LaNiO_3$ has shown clearly a renormalization of the Fermi velocity of e_g quasiparticles [19]. The spectroscopic evidence of strong correlations has triggered a theoretical calculation combining DFT and dynamical mean-field theory (DMFT) [36]. The calculation has given rise to a flatter dispersion curve than that from a DFT calcualtion. A factor three increase of $\gamma_{\rm cal}$ is still smaller than the γ obtained in this

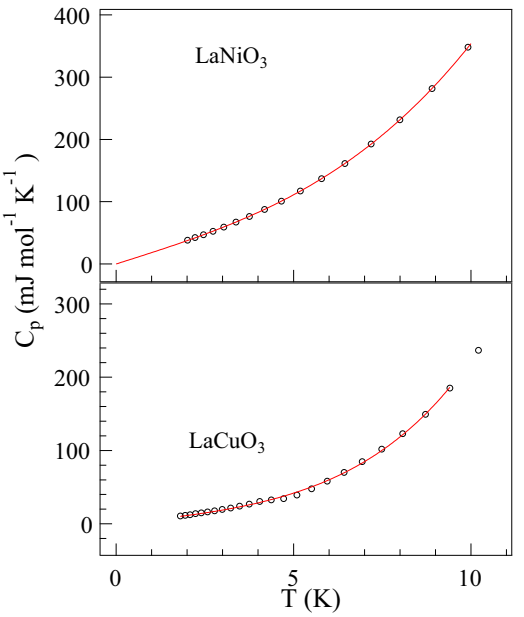

FIG. 5. (Color online) Temperature dependence of specific heat C_p at low temperatures for $LaNiO_3$ and $LaCuO_3$. Curves inside data points are the fitting results to the formula $C_p = \gamma T + \beta T^3 + \alpha T^5$.

work. The increased $\gamma_{\rm cal}$ and χ_0 based on the DFT+DMFT calculation would lower both the ratios of $\gamma/\gamma_{\rm cal}$ and χ/χ_0 for $LaNiO_3$ but not change the Stoner enhancement extracted from the ratio $(\chi/\chi_0)/(\gamma/\gamma_{\rm cal})$. The DFT+DMFT calculation makes us one step close to accounting for the complex correlation effect. It would be interesting to see similar spectroscopic work and the calculation on $LaCuO_3$.

The $3d$ band in transition-metal oxides is located between the cation $4s$ and the oxygen $2p$ bands. The $3d$ energies decrease towards the oxygen $2p$ band progressively from Ti^{3+} to Cu^{3+} in $LaMO_3$. A much enhanced covalent mixing between $3d$ and $2p$ in $LaNiO_3$ and $LaCuO_3$ as the charge transfer gap between the $3d$ band and the $2p$ band decreases broadens the bandwidth so as to make them metallic in the series of $LaMO_3$. $LaCoO_3$ would be located at the boundary of a localized to itinerant transition if Co^{3+} stays in the high spin state. Consistent with the experimental observation, this consideration would predict weaker correlations in $LaCuO_3$ than that in $LaNiO_3$.

After clearly identifying the Stoner enhancement in $LaNiO_3$, one may ask whether the Stoner enhancement in $LaNiO_3$ can be further increased so as to lead to a ferromagnetic instability as the bandwidth is tuned to fulfill the Stoner criterion. In order to answer this question, we need to review the well-established phase diagram of the $RNiO_3$ family in Fig. 7. $LaNiO_3$ is the only member in the family crystallized in the rhombohedral structure. As La is replaced by smaller rare earths R^{3+}, the structure becomes orthorhombic; there is an abrupt drop of the Ni-O-Ni bond angle on crossing the rhombohedral/orthorhombic structural transition, and the bond angle decreases further as the rare earth ionic size is reduced further in the orthorhombic phase. Therefore, the bandwidth of $LaNiO_3$ can be continuously reduced by substituting a smaller rare earth. Although the magnetic susceptibility is enhanced in $RNiO_3$ as R reduces [22], the enhancement does not result in a

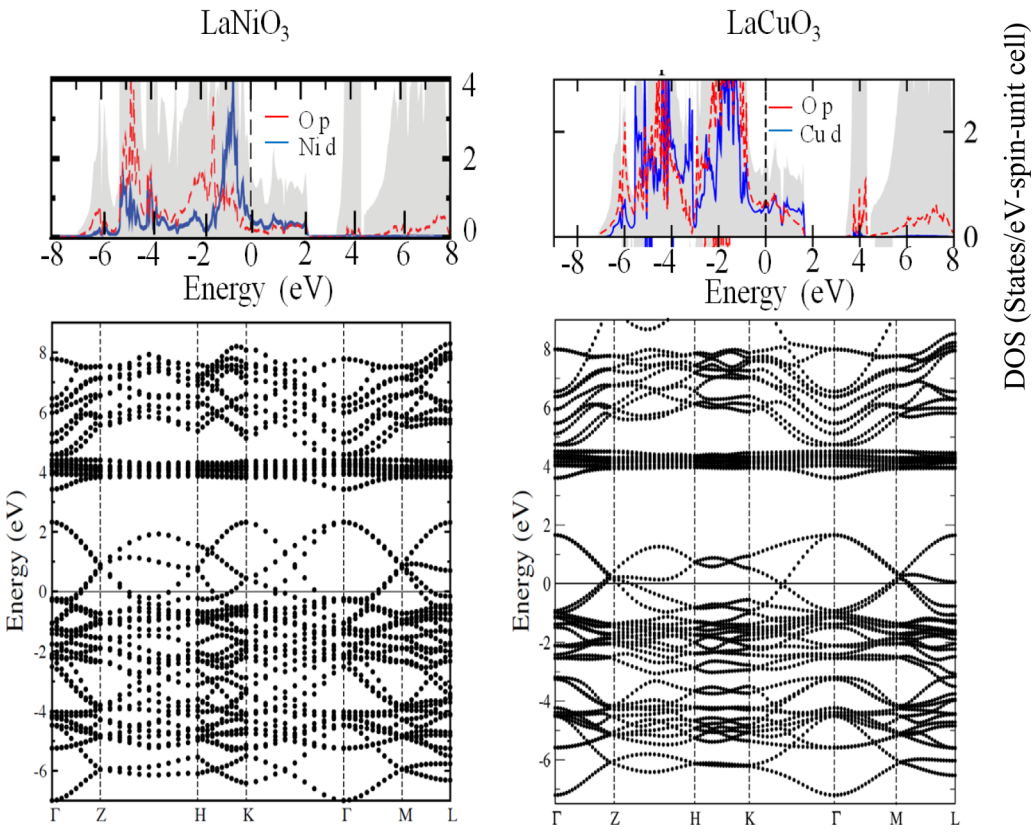

FIG. 6. (Color online) The band structure and DOS for $LaNiO_3$ and $LaCuO_3$ after Ref. [33]. The grey area indicates the total DOS.

ferromagnetic transition. Instead, the samples substituted with smaller rare earths end up with a type-E antiferromagnetic phase in the phase diagram of Fig. 7. Increasing U as the R reduces leads to a metal-insulator transition at T_{IM} in Fig. 7. Whereas the change of U would make the system close to the Stoner criterion in $RNiO_3$, the orbital ordering in the Mott insulator phase at $T < T_{IM}$ offers modulated exchange interactions, which leads to the spin ordering of up-up-down-down in the type E antiferromagnetic phase below T_N.

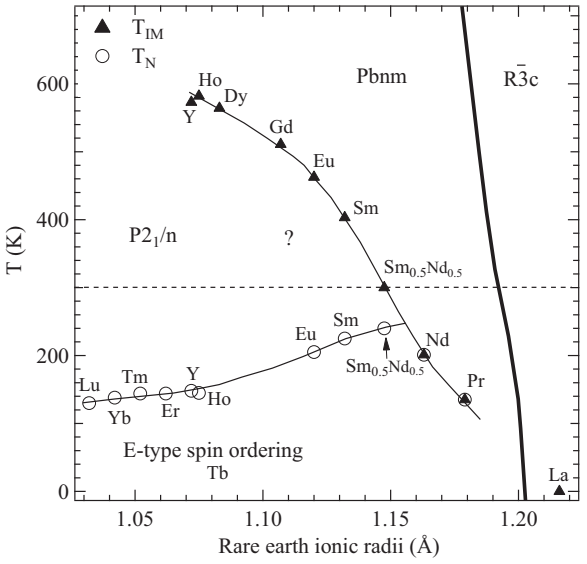

FIG. 7. Phase diagram of the $RNiO_3$ family.

Alternatively, the bandwidth of $LaNiO_3$ can possibly be reduced in a thin film grown epitaxially on a perovskite substrate with larger lattice parameter [37,38]. The lattice mismatch between $LaNiO_3$ and the substrate would place the thin film of $LaNiO_3$ under a tensile strain. Although the NiO_2 plane remains buckled, the Ni-O bond length is enlarged so that the bandwidth is reduced relative to that in the bulk sample. As shown by an optical study of a $LaNiO_3$ film on a $DyScO_3$ substrate [38], the effective mass, and therefore γ, is enhanced. Given a smaller sample volume, it is a challenge to determine whether the magnetic susceptibility of the film sample is even more enhanced than the electronic mass in the thin film sample.

The bandwidth of $LaNiO_3$ can be increased by applying hydrostatic pressure. As shown in the structural study of $LaCrO_3$ under pressure [29], while the Cr-O-Cr bond angle in the rhombohedral phase does not change obviously with pressure, the Cr-O bond length reduces continuously as pressure increases. We believe the high-pressure structure study of $LaCrO_3$ is applicable to the case of $LaNiO_3$. As shown in Fig. 2, pressure enhances the phonon-drag effect on the thermoelectric power at low temperatures. A weaker electron-phonon interaction under pressure implies that pressure broadens the bandwidth. The change of magnetic susceptibility under pressure tells directly whether the Stoner enhancement could be increased with pressure. Figure 8(a) shows the $\chi(T)$ of $LaNiO_3$ under different pressures. Pressure reduces χ at room temperature and makes χ more temperature dependent. As shown in Fig. 8, the temperature dependence of χ under different pressures can also be well fit by the formula

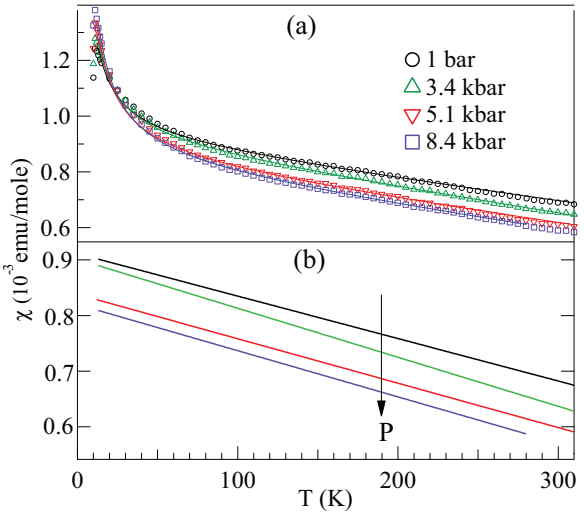

FIG. 8. (Color online) (a) Temperature dependence of the magnetic susceptibility for $LaNiO_3$ under different pressures; (b) the term $\chi_0(1-aT)$ in the curve fitting to $\chi = \chi_0(1-aT)+C/T$ in (a) under different pressures. The arrow inside (b) points to the direction of increasing pressure.

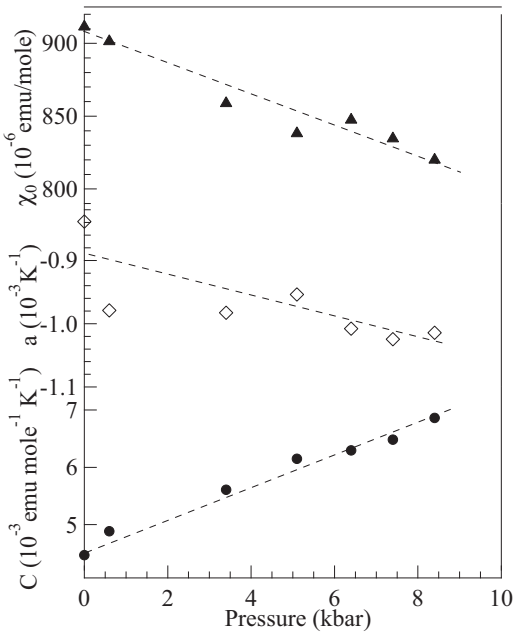

FIG. 9. Pressure dependence of fitting parameters in the formula for fitting the magnetic susceptibility under pressure; see the text for detailed information.

$\chi = \chi_0(1-aT)+C/T$. In order to see more clearly how the intrinsic magnetic property changes under pressure, we have isolated the term $\chi_0(1-aT)$ from $\chi = \chi_0(1-aT)+C/T$ under different pressure and plotted it in Fig. 8(b). The pressure dependence of fitting parameters is plotted in Fig. 9. The change of susceptibility from a phase with the Stoner enhancement to a phase with the Stoner instability should include two components: (a) a much increased χ at room temperature to a $\chi \sim 10^3$ emu/mole as seen in $ZrZn_2$ [39], and (b) a steeper slope in χ^{-1} versus T in order to apply the universal Curie-Weiss law [40] for the itinerant-electron ferromagnetism. Although χ of $LaNiO_3$ is enhanced relative to the DFT result, it is still smaller than the χ of $ZrZn_2$ by six orders. High pressure further reduces χ_0, so that pressure tunes the system away from the Stoner instability. As mentioned before, the Curie term C/T may be caused by impurities or defects. As χ_0 is reduced under pressure, the steeper temperature dependence of χ contributed from the C/T term becomes more pronounced. As a matter of fact, χ at the lowest temperature is nearly pressure independent. It is still not clear why the Curie term increases with pressure.

V. CONCLUSIONS

Results of new measurements together with those published previously on the same high-quality $LaNiO_3$ and $LaCuO_3$ samples have made it possible to extract the information of electron-electron correlations through bulk physical properties. By comparing quantitatively with the value from the DFT calculation, the renormalization at the Fermi energy due to correlations as represented in the γT term from the specific-heat measurement is clearly revealed in these narrowband metallic systems. An enhanced γ in $LaNiO_3$ has been nearly accounted for by the DFT+DMFT calculation. Depending on the band filling, spin fluctuations in a narrowband system give rise to a sharply different enhancement to the magnetic susceptibility. In the half-filled $LaCuO_3$, χ and γ are equally enhanced as predicted by Brinkman and Rice. In comparison, χ is much more enhanced in the quarter-filled $LaNiO_3$ than that for γ, indicating the Stoner enhancement. The band-filling factor is directly related to the sign of spin-spin interactions in a narrowband system, which is missed in the Stoner criterion. Although we have demonstrated the Stoner enhancement in $LaNiO_3$, the enhancement of χ does not lead to a Stoner instability by either narrowing or enlarging the bandwidth in the system.

ACKNOWLEDGMENT

This work was supported by National Science Foundation (Grant No. DMR1122603).

[1] N. F. Mott, *Metal-Insulator Transitions* (Taylor & Francis, London, 1990).
[2] G. Demazeau, A. Marbeuf, M. Pouchard, P. Hagenmuller, and J. B. Goodenough, C. R. Acad. Sci. **272**, 2163 (1971).
[3] G. Demazeau, C. Parent, M. Pouchard, and P. Hagenmuller, Mater. Res. Bull. **7**, 913 (1972).
[4] J. B. Goodenough, N. F. Mott, M. Pouchard, G. Demazeau, and P. Hagenmuller, Mater. Res. Bull. **8**, 647 (1973).
[5] J. F. Bringley, B. A. Scott, S. J. La Placa, R. F. Boehme, T. M. Shaw, M. W. McElfresh, S. S. Trail, and D. E. Cox, Nature (London) **347**, 263 (1990).
[6] D. B. Currie and M. T. Weller, Acta Crystallogr. Sec. C **47**, 696 (1991).

[7] S. Darracq, A. Largeteau, G. Demazeau, B. A. Scott, and J. F. Bringley, Eur. J. Solid State Inorg. Chem. **29**, 585 (1992).
[8] C. Weigl and K.-J. Range, J. Alloys Compd. **200**, L1 (1993).
[9] J.-H. Choy, D.-K. Kim, S.-H. Hwang, and G. Demazeau, Phys. Rev. B **50**, 16631 (1994).
[10] M. Karppinen, H. Yamauchi, H. Suematsu, K. Isawa, M. Nagano, R. Itti, and O. Fukunaga, J. Solid State Chem. **130**, 213 (1997).
[11] G. Yalovega and A. V. Soldatov, Phys. Status Solidi B **218**, 455 (2000).
[12] J.-S. Zhou, W. Archibald, and J. B. Goodenough, Phys. Rev. B **57**, R2017 (1998).
[13] J.-S. Zhou, W. Archibald, and J. B. Goodenough, Phys. Rev. B **61**, 3196 (2000).
[14] I. Presniakov, G. Demazeau, A. Baranov, A. Sobolev, T. Gubaidulina, and V. Rusakov, J. Solid State Chem. **180**, 3253 (2007).
[15] J. B. Torrance, P. Lacorre, A. I. Nazzal, E. J. Ansaldo, and Ch. Niedermayer, Phys. Rev. B **45**, 8209 (1992).
[16] K. Sreedhar, J. M. Honig, M. Darwin, M. McElfresh, P. M. Shand, J. Xu, B. C. Crooker, and J. Spalek, Phys. Rev. B **46**, 6382 (1992).
[17] X. Q. Xu, J. L. Peng, Z. Y. Li, H. L. Ju, and R. L. Greene, Phys. Rev. B **48**, 1112 (1993).
[18] M. L. Medarde, J. Phys.: Condens. Matter **9**, 1679 (1997).
[19] R. Eguchi, A. Chainani, M. Taguchi, M. Matsunami, Y. Ishida, K. Horiba, Y. Senba, H. Ohashi, and S. Shin, Phys. Rev. B **79**, 115122 (2009).
[20] R. D. Sánchez, M. T. Causa, A. Seoane, J. Rivas, F. Rivadulla, M. A. López-Quintela, J. J. Pérez Cacho, J. Blasco, and J. Garcia, J. Solid State Chem. **151**, 1 (2000).
[21] J.-S. Zhou, J. B. Goodenough, B. Dabrowski, P. W. Klamut, and Z. Bukowski, Phys. Rev. B **61**, 4401 (2000).
[22] J.-S. Zhou, J. B. Goodenough, B. Dabrowski, P. W. Klamut, and Z. Bukowski, Phys. Rev. Lett. **84**, 526 (2000).
[23] A. W. Webb, E. F. Skelton, S. B. Qadri, E. R. Carpenter, Jr., M. S. Osofsky, R. J. Soulen, and V. Letourneau, Phys. Lett. A **137**, 205 (1989).
[24] J.-S. Zhou, J. B. Goodenough, and B. Dabrowski, Phys. Rev. B **67**, 020404 (2003).
[25] J.-S. Zhou, J. B. Goodenough, and B. Dabrowski, Phys. Rev. Lett. **95**, 127204 (2005).
[26] T. P. Pearsall and C. A. Lee, Phys. Rev. B **10**, 2190 (1974).
[27] I. Nagai, N. Shirakawa, S. Ikeda, R. Iwasaki, H. Nishimura, and M. Kosaka, Appl. Phys. Lett. **87**, 024105 (2005).
[28] D. K. C. Macdonald, *Thermoelectricity: An Introduction to the Principles* (Wiley, New York, 1962).
[29] J.-S. Zhou, J. A. Alonso, A. Muoñz, M. T. Fernández-Díaz, and J. B. Goodenough, Phys. Rev. Lett. **106**, 057201 (2011).
[30] J.-G. Cheng, Y. Sui, J.-S. Zhou, J. B. Goodenough, and W. H. Su, Phys. Rev. Lett. **101**, 087205 (2008).
[31] P. Mohn, *Magnetism in the Solid State, An Introduction* (Springer, Berlin, 2006).
[32] For example, N. D. Mathur, F. M. Grosche, S. R. Julian, I. R. Walker, D. M. Freye, R. K. W. Haselwimmer, and G. G. Lonzarich, Nature (London) **394**, 39 (1998).
[33] J. He and C. Franchini, Phys. Rev. B **86**, 235117 (2012).
[34] A. L. Fetter and J. D. Walecka, *Quantum Theory of Many-Particle Systems* (Dover Publications, Inc, New York, 2003).
[35] W. F. Brinkman and T. M. Rice, Phys. Rev. B **2**, 4302 (1970).
[36] X. Deng, M. Ferrero, J. Mravlje, M. Aichhorn, and A. Georges, Phys. Rev. B **85**, 125137 (2012).
[37] M. K. Stewart, C.-H. Yee, J. Liu, M. Kareev, R. K. Smith, B. C. Chapler, M. Varela, P. J. Ryan, K. Haule, J. Chakhalian, and D. N. Basov, Phys. Rev. B **83**, 075125 (2011).
[38] D. G. Quellette, S.-B. Lee, J. Son, S. Stemmer, L. Balents, A. J. Millis, and S. J. Allen, Phys. Rev. B **82**, 165112 (2010).
[39] S. Ogawa and N. Sakamoto, J. Phys. Soc. Jpn. **22**, 1214 (1967).
[40] T. Moriya, *Electron Correlation and Magnetism in Narrow-Band Systems*, edited by T. Moriya, Springer Series in Solid-State Sciences 29 (Springer-Verlag, Berlin, 1981), p. 2.